Accepted Manuscript

Chemical and structural characterization of char development during lignocellulosic biomass pyrolysis

Lihle D. Mafu, Hein W.J.P. Neomagus, Raymond C. Everson, Christien A. Strydom, Marion Carrier, Gregory N. Okolo, John R. Bunt

PII: S0960-8524(17)31103-3
DOI: http://dx.doi.org/10.1016/j.biortech.2017.07.017
Reference: BITE 18436

To appear in: *Bioresource Technology*

Received Date: 24 May 2017
Revised Date: 3 July 2017
Accepted Date: 4 July 2017

Please cite this article as: Mafu, L.D., Neomagus, H.W.J., Everson, R.C., Strydom, C.A., Carrier, M., Okolo, G.N., Bunt, J.R., Chemical and structural characterization of char development during lignocellulosic biomass pyrolysis, *Bioresource Technology* (2017), doi: http://dx.doi.org/10.1016/j.biortech.2017.07.017

Chemical and structural characterization of char development during lignocellulosic biomass pyrolysis

Lihle D. Mafu[a], Hein W.J.P. Neomagus[a,b,‡], Raymond C. Everson[a,b], Christien A. Strydom[a] Marion Carrier[c], Gregory N. Okolo[b] and John R. Bunt[b]

[a]*Chemical Resource Beneficiation (CRB), School of Physical and Chemical Sciences, North-West University, Potchefstroom Campus, Private Bag X6001 Potchefstroom, 2520, South Africa*

[b]*School of Chemical and Minerals Engineering, Private Bag X6001, North-West University, Potchefstroom Campus, Potchefstroom 2520, South Africa*

[c]*Aston University, EBRI, Bioenergy Research Group, Birmingham B4 7ET, United Kingdom*

‡*hein.neomagus@nwu.ac.za*

Abstract

The chemical and structural changes of three lignocellulosic biomass samples during pyrolysis were investigated using both conventional and advanced characterization techniques. The use of ATR-FTIR as a characterization tool is extended by the proposal of a method to determine aromaticity, the calculation of both CH_2/CH_3 ratio and the degree of aromatic ring condensation ($(R/C)_u$). With increasing temperature, the H/C and O/C ratios, X_A and CH_2/CH_3 ratio decreased, while $(R/C)_u$ and aromaticity increased. The micropore network developed with increasing temperature, until the coalescence of pores at 1100 °C, which can be linked to increasing carbon densification, extent of aromatization and/or graphitization of the biomass chars. WAXRD-CFA measurements indicated the gradual formation of nearly parallel basic structural units with increasing carbonization temperature. The char development can be considered to occur in two steps: elimination of aliphatic compounds at low temperatures, and hydrogen abstraction and aromatic ring condensation at high temperatures.

***Keywords**: Aromaticity, ATR-FTIR, biochar, CPMAS ^{13}C NMR, pyrolysis*

1 Introduction

Interest in the use of biomass for energy generation has grown considerably in recent years, since it is considered to be a more sustainable alternative to fossil fuels (Mao et al., 2015; Pimenidou and Dupont, 2012). One process of ensuring the efficient use of biomass in energy production is pyrolysis, where fast pyrolysis is often preferred for liquid products and low heating rates are used for the production of chars (Fisher et al., 2012). The biomass origin and the pyrolysis conditions such as heating rate, pyrolysis temperature and gas environment shape the chemical and structural characteristics of the formed chars (Rutherford et al., 2012; Wei et al., 2011). The transformation of a broad range of plant biomass sources resulted in the production of carbonaceous material displaying properties suitable for various applications such as soil amendment, gasification and co-gasification with coal (Angin and Sensoz, 2014; Kaudal et al., 2016). In addition to variable lignocellulosic composition, the presence of inorganic compounds results in peculiar reactivity of plant biomass during pyrolysis, gasification and combustion. For example, feedstocks with a high mineral matter content may be preferred for co-gasification applications due to a favourable catalytic effect of the specific minerals (Huang et al., 2009). On the other hand, low ash feedstocks may be directly transformed into liquids that should result in more stable biofuels (Antonio et al., 2014).

The intended application of pyrolytic chars is dependent on their structural and chemical characteristics, which is in turn reliant on the pyrolysis conditions. For instance, chars produced at higher temperatures have shown higher fixed carbon and elemental carbon, lower volatile matter, lower elemental oxygen and hydrogen contents (Uzun et al., 2006; Zhang et al., 2016). A number of advanced techniques has been developed and used to provide more information on the changes in characteristics induced by pyrolysis (Rutherford et al., 2012; Suliman et al., 2016). Wide angle X-ray diffraction – carbon fraction analysis (WA-XRD-CFA) has been useful in identifying the phases of biomass and has been extended to evaluating the microcrystalline parameters (Huang et al., 2009). This has been done by the determination of the interlayer spacing (d_{002}), crystalline height (L_c), crystalline diameter (L_a) and the average number of aromatic layers per carbon crystallite (N_{ave}) using the Bragg's and Scherrer's equation (Okolo et al., 2015). The transformation of the surface functionalities, or functional groups, as biomass undergoes heat treatment, has been studied by Fourier Transforms infrared (FTIR) spectroscopy. Major findings include the elimination of aliphatic groups at lower temperatures and as heating temperatures were increased, the aromatic

functional groups lost their infrared activity resulting in a spectrum with no FTIR peaks (Rutherford et al., 2012; Suliman et al., 2016). Cui et al. (2016) used FTIR to extract coal structural parameters which included the fraction of aromatic and aliphatic fractions. It was concluded that the CH_2/CH_3 ratio increased with coal rank, pyrolysis temperature and pyrolysis time. Most findings from FTIR have been complemented by results from cross polarization magnetic angle spinning nuclear magnetic resonance (CPMAS ^{13}C NMR) spectroscopy and surface area measurements (McBeath et al., 2011; Suliman et al., 2016).

In addition, the characterization techniques have revealed important details in the process of char formation, which depends on the pyrolysis conditions and biomass characteristics. The lignocellulosic fibre composition has been reported to be the basis of observed chemical and structural changes during low temperature pyrolysis (Mafu et al., 2016; Wannapeera and Worasuwannarak, 2012). At temperatures above 500 °C, the vast majority of fibres have been found to be consumed through decomposition.

When considering processing conditions in a typical fixed bed dry bottom (FBDB) gasifier, the pyrolysis zone may rise up to temperatures above 1000 °C, while the heating rate is relatively low (10 – 20 ^{o}C/min) (Skhonde et al., 2009) and as such, the understanding of slow pyrolysis char formation even up to higher temperatures is justified. The characteristics of chars produced from the pyrolysis zone affect the gasification kinetics during biomass gasification or co-gasification with coal (Kajitani et al., 2010; Y. Zhang et al., 2016). It has been reported that the aromaticity, for instance, is a function of charring temperature (Everson et al., 2013), which increases with increasing pyrolysis temperature, while the gasification reactivity of the formed char has been shown to decrease with increasing aromaticity. However, as aromatization progresses, other chemical transformations that affect the crystallinity, the surface area and the microcrystalline structure are simultaneously taking place. The progress of char formation in slow pyrolysis, together with correlations between the various char characteristics have not yet received significant attention, and forms the motivation of this study.

The chemical and structural characterization of biomass, similar to coal, provides insight in the thermal behaviour, such as the gasification reactivity. As such, this work reports on the slow pyrolysis char development in the region of torrefaction to gasification temperatures. The effect of temperature on three different biomass samples that are widely available in South Africa is discussed, and outcomes include: the determination of aromaticity (f_{aF}), degree of aromatic ring condensation ($(R/C)_u$), and aliphatic CH_2/CH_3 ratios from ATR-FTIR

spectroscopy data; fraction of amorphous carbon (X_A) and Van Krevelen plots of the samples. From the reported results, the char development is then explained using both chemical and structural characteristics by relating aromaticity to other char characteristics, which has been an area that is inadequately explored in biomass studies.

2 Materials and Methods

2.1 Materials

Three abundantly available biomass sources in South Africa were procured. Softwood (SW) and hardwood (HW) chips were supplied by South African Pulp and Paper Industries Limited (SAPPI), whereas sweet sorghum bagasse (SB) was obtained from the Agricultural Research Council (ARC) in Potchefstroom. Approximately 10 kg of each sample was obtained and air-dried overnight. Successively, the sample size was representatively reduced by applying a standardised cone and quartering method (DD CEN/TS 14780:2005) three times. The obtained sample was ground to < 300 µm and was further used for characterisation and conversion experiments. From the bulk samples, about 15 g of the air-dried and ground biomass samples were heated at 10 °C/min using a N_2 gas flow rate of 100 ml/min from room temperature to 260 °C in a tube furnace from Elite Thermal Systems Limited (Model TSH12/75/610) to achieve a 30% mass loss. The changes in characteristics after torrefaction are reported in a previous study (Mafu et al., 2016). Chars for this study were prepared from the torrefied biomass, in the same furnace by heating at 10 °C/min to final temperatures of 300, 400, 600 and 1100 °C and left isothermal for 60 minutes. The series of pyrolytic chars were referred to by the plant biomass that they were produced from, and the highest temperature of the pyrolysis treatment (e.g. softwood char prepared at 300 °C is referred to as SW 300).

2.2 Characterization

Ultimate analysis was carried out by means of the standard ASTM D 5373 method for elemental C, H and N, whilst the elemental S and O mass percentages were determined by the ASTM D 4239 method and by difference, respectively. The volatile matter and mineral matter contents were obtained using the ISO 562:2010 and ISO 1171:2010 methods respectively, whilst the fixed carbon content was calculated by difference. Both analyses were carried out by the Council of Geosciences, Pretoria, South Africa. Infrared spectra were recorded using a Perkin–Elmer Paragon 1000 PC Fourier Transforms Infrared (FTIR) spectrometer with an attenuated total reflectance (ATR) accessory between 400 and 4000 cm^-

^{1} with 4 cm^{-1} resolution, where 32 scans were averaged for one sample run. CPMAS ^{13}C NMR experiments were carried out at the Central Analytical Facility of Stellenbosch University following the method by Melkior et al. (2012), which involves a combination of cross polarization and magnetic angle spinning techniques. A Quanta FEG 250 Environmental Scanning electron microscope (ESEM) under an acceleration voltage of 30 kV was used to capture the surface morphology of biomass char samples and the imaging was improved by lightly covering the sample with a gold layer at the Laboratory of Electron Microscopy (LEM) of the North-West University. WA-XRD-CFA was conducted at the North-West University following a method outlined in Mafu et al. (2016). Surface area measurements were obtained from a Micrometrics ASAP 2020 surface area and porosity analyser. Samples were degassed under vacuum, at 75 °C for 48 h and analysis conducted at 0 °C at a relative pressure range: $0 < P/P_0 \leq 0.032$: where P is the analysis pressure and P_0 is the saturation vapour pressure of CO_2. The Dubinin-Radushkevich (D-R) and Horvath-Kawazoe (H-K) models were used to obtain the micropore surface area, maximum pore volume and median pore width (Okolo et al., 2015).

From ATR-FTIR spectroscopy, the sum of aromatic functional groups and the sum of aliphatic functional groups, derived by Gaussian curve deconvolution, were used to calculate the aromaticity. The aromaticity ($f_{a,F}$), defined as the fraction of aromatic groups from the sum of aliphatic and aromatic groups in the sample is given by Equation 1. The aromaticity values from this proposed method were compared to those determined from CPMAS ^{13}C NMR ($f_{a,N}$). The $f_{a,F}$ was then used to calculate the degree of aromatic ring condensation (Equation 2) which was found to be proportional to the total aromaticity ($f_{a,F}$ in this case) and the fraction of aromatic hydrogen (H_{ar}) to aromatic carbon (C_{ar}) by Cui et al., (2016). The asymmetric stretching of CH_3 and CH_2 groups have been used as an indication of the degree of cyclization, where a higher value of CH_2/CH_3 revealed longer aliphatic chains or a higher degree of cyclization. The value of CH_2/CH_3 was determined using Equation 3 where A_{2925} and A_{2955} represent the area under the deconvoluted curves of ATR-FTIR peaks at 2925 and 2955 cm^{-1}, respectively. The fraction of amorphous carbon, X_A, was determined by the Gaussian curve deconvolution of the amorphous and crystalline phases of the 002 band of the XRD spectra (Figure 1). The area under the curve at position 16° and 25° after deconvolution were assigned to the amount of amorphous carbon (S_A) and crystalline carbon (S_C), respectively. X_A was calculated using Equation 4 (Okolo et al., 2015). Using the empirical Bragg's and Scherrer's equations, the crystallite height (L_c), crystallite diameter (L_a),

interlayer spacing (d_{002}) and average number of aromatic layers per carbon crystallite (N_{ave}) were calculated (Everson et al., 2013; Okolo et al., 2015).

$$f_{aF} = \frac{\sum C_{ar}}{\sum C_{ar+al}} \quad (1)$$

$$\left(\frac{R}{C}\right)_u = 1 - \frac{1}{2}\left(f_a + \frac{H_{ar}}{C_{ar}}\right) \quad (2)$$

$$\frac{CH_2}{CH_3} = \frac{A_{2925/cm}}{A_{2955/cm}} \quad (3)$$

$$X_A = \frac{S_A}{S_A + S_C} \quad (4)$$

3 Results and discussion

3.1 Chemical characteristics

Table 1 presents the chemical characteristics of the pyrolytic chars. Char development progressed with increasing temperature through the evolution of volatiles, which results in increased fixed carbon and mineral matter contents. The proximate analyses showed minor changes between torrefied biomass and chars prepared at 300 °C. Further changes up to 600 °C were linked to the decomposition of cellulose and lignin (Giudicianni et al., 2013). The differences in proximate analyses chars prepared at 600 and 1100 °C were significant and reported to be mainly driven by secondary reactions (Anca-Couce, 2016). The calorific value (CV) increased with increasing pyrolysis temperature, but decreased at 1100 °C for all biomass samples. The increase in CV at lower temperatures is attributed to the reduction in elemental O and H, and increasing carbon content (carbon densification) in the solid matrix. However, the graphitization of the solid mass at high temperatures accounts for the reduction in CV for the for the 1100 °C chars, as observed for coal (Suggate and Dickinson, 2004). Increasing pyrolysis temperature resulted in the increase in elemental carbon, whilst elemental oxygen and hydrogen decreased appreciably. Noteworthy were the larger changes in ultimate analysis results from torrefied biomass to chars prepared at 600 °C as a result of the degradation of lignocellulosic fibres (Yang et al., 2006). Beyond 600 °C, changes were a result of bond reordering and hydrogen abstraction as shown by further decreases in elemental H and O (Trubetskaya et al., 2016a). The amounts of N and S were very low; as

such no trends could be drawn. The changes in C, H and O amounts result in the reduction of the H/C and O/C ratios linked to an increase in aromaticity (Anupam et al., 2016). The decrease of H/C and O/C ratios as shown in the Van Krevelen plot (Figure 2) with temperature was comparable to the coalification process with torrefied biomass' ratios similar to those of peat and chars prepared at 1100 °C to anthracite coals (Anupam et al., 2016; Suggate and Dickinson, 2004).

ATR-FTIR spectra for chars prepared at 1100 °C could not be collected due to line broadening and absence of vibrating and stretching functional groups at high temperatures (Roberts et al., 2015; Rutherford et al., 2012). Torrefied biomass displayed characteristic vibrations corresponding to the presence of aliphatic groups (3200-3500, 2800-3000 and 900-1150 cm^{-1}) and aromatic groups (700-900, 1150-1650 cm^{-1}) (Huang et al., 2015; Zhao et al., 2013) which can be attributed to the presence of residual lignocellulosic fibres (Anca-Couce, 2016; Pimenidou and Dupont, 2012).

The deconvoluted area under the aromatic ATR-FTIR peaks could not be related to the amounts of lignin at torrefaction conditions (Mafu et al., 2016), but from both aliphatic and aromatic peaks, the aromaticity of the materials could be determined. SB had the lowest aromaticity of the torrefied biomass samples, due to the lower lignin contents in the parent biomass, compared to SW and HW (Mafu et al., 2016). Aromaticity increased with increasing pyrolysis temperature (Table 2) as alluded to previously by other researchers (Asadullah et al., 2010; McBeath et al., 2011). The observed increase in aromaticity had two contributing factors: (1) the elimination of aliphatic groups taking place more rapidly than the loss of aromatics and (2) the condensation of aromatic rings as observed by the increase in $(R/C)_u$ with increasing pyrolysis temperature (Table 2). The parameter, CH_2/CH_3 ratio, was determined and the results are presented in Table 2. For torrefied biomass samples, the CH_2/CH_3 ratio was around 50 and decreased with increasing temperature to approximately 1 for chars prepared at 600 °C. This could be a consequence of progressing cyclization of the aliphatics, as well as the shorter $–CH_2$ aliphatic chains being easily broken compared to the longer $–CH_3$ aliphatic chains (Cui et al., 2016). Functionalities containing elemental H and O gradually decreased at pyrolysis temperatures up to 300 °C as a result of dehydration (Rutherford et al., 2012). Subsequent elimination of aliphatic functionalities, H- and O-containing functional groups up to 600 °C could be related to the degradation of fibre components (Yang et al., 2013) and was consistent with the ultimate analysis data (Table 1).

From CPMAS ^{13}C NMR spectroscopy, the presence of acetyl, methoxyl, amorphous and crystalline carbons of cellulose and aromatic groups of lignin in all biomass samples could be confirmed by the presence of peaks at characteristic positions (Freitas et al., 2001; Mafu et al., 2016). For chars prepared at 300 °C, peaks related to hemicelluloses and amorphous carbons of cellulose and lignin, gradually decreased as a result of the degradation of the lignocellulosic fibres. Peaks at 35, 68, 62, 65, 73, 84, 105, 112 and 149 ppm were visible for chars at 300 °C and related to the carbons of the crystalline cellulose and lignin (Bardet et al., 2007; Melkior et al., 2012). Shoulder peaks at 62-65 ppm and 72-74 ppm were as a result of residual amorphous carbons (Mafu et al., 2016). At 400 °C, the peak areas of characteristic cellulose and lignin peaks reduced, as a result of the reduction of their carbon functionalities (Rutherford et al., 2012). Chars prepared at 600 °C had mainly aromatic carbon functionalities with fractions of amorphous C=C and C-H left in the chars. The differences between woody biomass and SB were more significant for chars prepared at 300 °C, and converged to almost the same ^{13}C chemical structure at 600 °C, which was also observed by McBeath et al., (2011) for different lignocellulosic biomass samples. These findings suggests that char development may be broadly defined as a two-step process, where the first step (< 600 °C) is accompanied by lignocellulosic fibre degradation linked to the net loss of the aliphatic fraction of biomass. The second step (> 600 °C) may be assigned to the reorganisation of bonds that result in the conjugation of aromatic bonds, hence increasing further, the aromaticity of chars. The aromaticity as determined through both ATR-FTIR and NMR were comparable as presented in Table 2.

3.2 Structural characteristics

Due to the insignificant changes as pyrolysis temperatures were increased to 1100 °C, only torrefied, 300 and 1100 °C char micrographs are presented and discussed. The surface for all torrefied biomass was smooth, possibly from the melting of lignin and cellulose (Mafu et al., 2016). With increasing temperature, the matrix did not change but rather became brittle (Cetin et al., 2004), that is, the escape of volatiles left a rigid, hollow biomass matrix (Trubetskaya et al., 2016a). A slight broadening of the water conducting pores was also observed for all biomass samples with increasing pyrolysis temperature (Liu et al., 2010; Trubetskaya et al., 2016a).

The diffractograms showed two broad and distinct peaks at the 2θ positions 16 and 25° assigned to amorphous and graphitic basal planes, respectively. Most of the crystalline carbon in biomass is in general ascribed to the presence of cellulose, whilst the other lignocellulosic

fibres contribute to the amorphous carbon content (Barnette et al., 2012; Murillo et al., 2014). The intensities of both peaks were lesser for SB than HW and SW, which was a direct consequence of the higher amount of mineral matter and lower content in original lignocellulosic fibres in SB than HW and SW (Mafu et al., 2016). As the pyrolysis temperature increased, the amorphous carbon peak (16°) progressively disappeared, in line with the degradation of hemicelluloses and other amorphous fractions of biomass. The crystalline phase narrowed as the temperature increased from 300 to 600 °C, following the degradation of celluloses at these conditions (Tumuluru et al., 2011; Yang et al., 2007). Chars prepared at 1100 °C showed increased peak intensity at 27° which may be a result of the recrystallization of some of the carbon material in the matrix (Azargohar et al., 2014). Increasing pyrolysis temperature promoted structural orderliness within the residual solid matrix as illustrated by the shift of the (002) band towards higher angle (2θ) regions (25 – 28°). The emergence of sharp peaks at 52 and 60° reflected the increasing share of minerals such as oxides and carbonates of Si, Mg and Ca (Trubetskaya et al., 2016b; Wen et al., 2014).

CO_2 adsorption results showed an increase in the micropore surface area with increasing pyrolysis temperature up to 600 °C (Table 3). This occurred through the development of micropores, with increasing micropore volume as volatiles were increasingly driven off, facilitated by carbon densification in the bulk biomass char. At 1100 °C, both micropore surface area and micropore volumes decreased for SW and SB. This was ascribed to pore coalescence at higher temperatures (Angin and Sensoz, 2014; Mukome et al., 2013). Pyrolytic chars prepared from HW at 1100 °C were an exception as they demonstrated an increase in the surface area and pore volume (Table 3). This could be a consequence of the accumulation of pores in the higher micropore range without a disruption of the lower micropore range, which was not the case for SB and SW. The lower pore volumes, and consequently surface areas of SB compared those of the woody biomass samples may be as a result of the higher ash values which may hinder pore development and/or block the access of pores by CO_2 (Tumuluru et al., 2011). There were no significant changes in the average pore diameter as the pyrolysis temperature increased. They ranged from 3.5-4.1 Å for all biomass samples suggesting that pore development happens through the formation of channels with deeper pores (Mafu et al., 2016).

The structural lattice parameters and fraction of amorphous carbon, X_A, are presented in Table 3. The different torrefied biomass samples showed approximately the same amounts (fractions) of amorphous carbon. The determined X_A was reported as being representative of

the amorphous sections of the fibres, which were not degraded during heat treatment (Mafu et al., 2016). Pyrolytic chars of SB were more sensitive to heat owing to the limited shielding by the lower lignin contents in SB compared to HW and SW. At 600 °C, X_A could not be determined by means of WA-XRD-CFA for SB char, while this was observed only at 1100 °C for HW and SW chars. As the pyrolysis temperature increased, d_{002}, L_c and N_{ave} decreased significantly, whilst L_a was considerably increased. The reduction in d_{002} resulted in the decrease of L_c producing a more packed microcrystallite lattice. Thus, the carbon crystallite of the biomass chars were significantly stretched in the y-direction resulting in flat layered carbon sheets. The average number of crystallites in a stack was reduced as d_{002} and L_c decreased. These lattice parameter changes may indicate changes of the micropore network. From 600 °C, the structural parameters of woody biomass became more similar to each other and increasingly different from that of the bagasse sample. This may be a consequence of the rearrangement reactions that dominate char formation at high temperatures (Trubetskaya et al., 2016a).

The extracted characteristics of biomass and subsequent chars were correlated with their H/C ratios as presented in Figure 3 (a – c). Inverse linear correlations were observed between the H/C ratios and the aromaticity (Figure 3(a)), and the degree of aromatic ring condensation, $(R/C)_u$, of the chars as shown in Figure 3(b). This implies that both the aromaticity and $(R/C)_u$ can be predicted from the empirical H/C ratios, following the correlation equations shown in Table 4, with correlation coefficients > 0.98. Conversely, the CH_2/CH_3 ratio was found to increase with increasing H/C ratio (equivalent to decreasing aromaticity) as presented in Figure 3(c) with a power law fitting. It has been demonstrated that the CH_2/CH_3 ratios of the chars can as well, be estimated from the H/C ratios of the studied samples from the correlation equations given in Table 4. Thus, with increasing pyrolysis temperature, char development proceeds by the elimination of aliphatic groups while aromaticity increases, complemented by the progression of aromatic ring condensation, $(R/C)_u$, with the concomitant hydrogen abstraction. These processes, coupled with increasing carbon densification of the biomass chars, also impacted the pore structure evolution and development. For example, the micropore surface area as shown in Figure 6(d) and the micropore volume (Table 3) increased with increasing with increasing pyrolysis temperature up to 600 °C. This may be linked to the elimination of aliphatic chains and the escape of volatiles leaving behind pores as the pyrolysis temperature increased. However, pore coalescence was observed for char samples of SW and SB at 1100 °C, similar to reported

findings for coal (Roberts et al., 2015). From these established correlations, it is evident that the charring process is a combination of aliphatics elimination and the aromatic ring condensation which results in the gradual increase in aromaticity with increasing temperature.

4 Conclusions

Char development was found to be dependent on the pyrolysis conditions. There was an observed link between the proximate and ultimate analysis data with fibre degradation. Chemical properties of the chars can be extracted from ATR-FTIR data, complimenting results from other techniques. Gradual decrease in H/C and O/C ratios, and aliphatic chains with increasing pyrolysis temperature, resulted in increasing f_a and $(R/C)_u$ of the chars. While micropore development was observed up to 600 °C, pore coalescence was more significant for SW and SB at 1100 °C. Char development can be considered as a two steps process: < 600 °C where changes were attributed to fibre degradation, resulting in the removal of aliphatics, and > 600 °C where changes were as a result of hydrogen abstraction and aromatic ring condensation.

Acknowledgments

The work presented in this paper is based on the research financially supported by the South African Research Chairs Initiative of the Department of Science and Technology (DST) and National Research Foundation (NRF) of South Africa (Coal Research Chair Grant Nos. 86880, UID85643, UID85632). Any opinion, finding or conclusion or recommendation expressed in this material is that of the author(s) and the NRF does not accept any liability in this regard.

Appendix A

Supplementary data associated with this article can be found, in the online version, at

References

1. Anca-Couce, A., 2016. Reaction mechanisms and multi-scale modelling of lignocellulosic biomass pyrolysis. Prog. Energy Combust. Sci. 53, 41–79.
2. Angin, D., Sensoz, S., 2014. Effect of Pyrolysis Temperature on Chemical and Surface Properties of Biochar of Rapeseed (*Brassica napus L.*). Int. J. Phytoremediation 16, 684–693.
3. Antonio, W., Lenço, P.C., Carvalho, D.J., Paulo, J., Veiga, S., 2014. The generation of residual biomass during the production of bio-ethanol from sugarcane , its characterization and its use in energy production. Renew. Sustain. Energy Rev. 29,

589–603.

4. Anupam, K., Sharma, A.K., Lal, P.S., Dutta, S., Maity, S., 2016. Preparation, characterization and optimization for upgrading *Leucaena leucocephala* bark to biochar fuel with high energy yielding. Energy 106, 743–756.
5. Asadullah, M., Zhang, S., Min, Z., Yimsiri, P., Li, C.-Z., 2010. Effects of biomass char structure on its gasification reactivity. Bioresour. Technol. 101, 7935–43.
6. Azargohar, R., Nanda, S., Kozinski, J.A., Dalai, A.K., Sutarto, R., 2014. Effects of temperature on the physicochemical characteristics of fast pyrolysis bio-chars derived from Canadian waste biomass. Fuel 125, 90–100.
7. Bardet, M., Hediger, S., Gerbaud, G., Gambarelli, S., Jacquot, J.F., Foray, M.F., 2007. Investigation with ^{13}C NMR , EPR and magnetic susceptibility measurements of char residues obtained by pyrolysis of biomass. Fuel 86, 1966–1976.
8. Barnette, A.L., Lee, C., Bradley, L.C., Schreiner, E.P., Bum, Y., Shin, H., Cosgrove, D.J., Park, S., Kim, S.H., 2012. Quantification of crystalline cellulose in lignocellulosic biomass using sum frequency generation (SFG) vibration spectroscopy and comparison with other analytical methods. Carbohydr. Polym. 89, 802–809.
9. Cetin, E., Moghtaderi, B., Gupta, R., Wall, T.F., 2004. Influence of pyrolysis conditions on the structure and gasification reactivity of biomass chars. Fuel 83, 2139–2150.
10. Cui, T., Fan, W., Dai, Z., Guo, Q., Yu, G., Wang, F., 2016. Variation of the coal chemical structure and determination of the char molecular size at the early stage of rapid pyrolysis. Appl. Energy 179, 650–659.
11. Everson, R.C., Okolo, G.N., Neomagus, H.W.J.P., Santos, J., 2013. X-ray diffraction parameters and reaction rate modeling for gasification and combustion of chars derived from inertinite-rich coals. Fuel 109, 148–156.
12. Fisher, E.M., Dupont, C., Darvell, L.I., Commandré, J.M., Saddawi, a., Jones, J.M., Grateau, M., Nocquet, T., Salvador, S., 2012. Combustion and gasification characteristics of chars from raw and torrefied biomass. Bioresour. Technol. 119, 157–165.
13. Freitas, J.C.C., Bonagamba, T.J., Emmerich, F.G., 2001. Investigation of biomass-and polymer-based carbon materials using ^{13}C high-resolution solid-state NMR. Carbon. 39, 535–545.
14. Giudicianni, P., Cardone, G., Ragucci, R., 2013. Cellulose , hemicellulose and lignin slow steam pyrolysis : Thermal decomposition of biomass components mixtures. J.

Anal. Appl. Pyrolysis 100, 213–222.

15. Huang, L., Chen, Y., Liu, G., Li, S., Liu, Y., Gao, X., 2015. Non-isothermal pyrolysis characteristics of giant reed (*Arundo donax L.*) using thermogravimetric analysis. Energy 87, 31–40.
16. Huang, Y., Yin, X., Wu, C., Wang, C., Xie, J., Zhou, Z., Ma, L., Li, H., 2009. Effects of metal catalysts on CO_2 gasification reactivity of biomass char. Biotechnol. Adv. 27, 568–72.
17. Kajitani, S., Zhang, Y., Umemoto, S., Ashizawa, M., Hara, S., 2010. Co-gasification reactivity of coal and woody biomass in high-temperature. Energy & Fuels 24, 145–151.
18. Kaudal, B.B., Chen, D., Madhavan, D.B., Downie, A., Weatherley, A., 2016. An examination of physical and chemical properties of urban biochar for use as growing media substrate. Biomass and Bioenergy 84, 49–58.
19. Liu, Z., Zhang, F., Wu, J., 2010. Characterization and application of chars produced from pinewood pyrolysis and hydrothermal treatment. Fuel 89, 510–514.
20. Mafu, L.D., Neomagus, H.W.J.P., Everson, R.C., Carrier, M., Strydom, C.A., Bunt, J.R., 2016. Structural and chemical modifications of typical South African biomasses during torrefaction. Bioresour. Technol. 202, 192–197.
21. Mao, Y., Dong, L., Dong, Y., Liu, W., Chang, J., Yang, S., Lv, Z., Fan, P., 2015. Fast co-pyrolysis of biomass and lignite in a micro fluidized bed reactor analyzer. Bioresour. Technol. 181, 155–162.
22. McBeath, A. V, Smernik, R.J., Schneider, M.P.W., Schmidt, M.W.I., Plant, E.L., 2011. Determination of the aromaticity and the degree of aromatic condensation of a thermosequence of wood charcoal using NMR. Org. Geochem. 42, 1194–1202.
23. Melkior, T., Jacob, S., Gerbaud, G., Hediger, S., Pape, L. Le, Bonnefois, L., Bardet, M., 2012. NMR analysis of the transformation of wood constituents by torrefaction. Fuel 92, 271–280.
24. Mukome, F.N.D., Zhang, X., Silva, L.C.R., Six, J., Parikh, S.J., 2013. Use of chemical and physical characteristics to investigate trends in biochar feedstocks. J. Agric. Food Chem. 61, 2196–2204.
25. Murillo, J.D., Ware, E.A., Biernacki, J.J., 2014. Characterization of milling effects on the physical and chemical nature of herbaceous biomass with comparison of fast pyrolysis product distributions using Py-GC/MS. J. Anal. Appl. Pyrolysis 108, 234–247.

26. Okolo, G.N., Neomagus, H.W.J.P., Everson, R.C., Roberts, M.J., Bunt, J.R., Sakurovs, R., Mathews, J.P., 2015. Chemical–structural properties of South African bituminous coals: Insights from wide angle XRD–carbon fraction analysis, ATR–FTIR, solid state ^{13}C NMR, and HRTEM techniques. Fuel 158, 779–792.
27. Pimenidou, P., Dupont, V., 2012. Characterisation of palm empty fruit bunch (PEFB) and pinewood bio-oils and kinetics of their thermal degradation. Bioresour. Technol. 109, 198–205.
28. Roberts, M.J., Everson, R.C., Neomagus, H.W.J.P., Okolo, G.N., Van Niekerk, D., Mathews, J.P., 2015. The characterisation of slow-heated inertinite- and vitrinite-rich coals from the South African coalfields. Fuel 158, 591–601.
29. Rutherford, D.W., Wershaw, R.L., Rostad, C.E., Kelly, C.N., 2012. Effect of formation conditions on biochars : Compositional and structural properties of cellulose , lignin , and pine biochars. Biomass and Bioenergy 46, 693–701.
30. Skhonde, M.P., Matjie, R.H., Bunt, J.R., Strydom, A.C., Schobert, H., 2009. Sulfur Behavior in the Sasol-Lurgi Fixed-Bed Dry-Bottom Gasification process. Energy & Fuels 23, 229–235.
31. Suggate, R.P., Dickinson, W.W., 2004. Carbon NMR of coals: The effects of coal type and rank. Int. J. Coal Geol. 57, 1–22.
32. Suliman, W., Harsh, J.B., Abu-Lail, N.I., Fortuna, A.M., Dallmeyer, I., Garcia-Perez, M., 2016. Influence of feedstock source and pyrolysis temperature on biochar bulk and surface properties. Biomass and Bioenergy 84, 37–48.
33. Trubetskaya, A., Jensen, P.A., Jensen, A.D., Garcia Llamas, A.D., Umeki, K., Glarborg, P., 2016a. Effect of fast pyrolysis conditions on biomass solid residues at high temperatures. Fuel Process. Technol. 143, 118–129.
34. Trubetskaya, A., Jensen, P.A., Jensen, A.D., Steibel, M., Spliethoff, H., Glarborg, P., Larsen, F.H., 2016b. Comparison of high temperature chars of wheat straw and rice husk with respect to chemistry, morphology and reactivity. Biomass and Bioenergy 86, 76–87.
35. Tumuluru, J.S., Sokhansanj, S., Hess, J.R., Wright, C.T., Boardman, R.D., 2011. A review on biomass torrefaction process and product properties for energy applications. Ind. Biotechnol. 7, 384–402.
36. Uzun, B.B., Putun, A.E., Ersan, P., 2006. Fast pyrolysis of soybean cake : Product yields and compositions. Bioresour. Technol. 97, 569–576.
37. Wannapeera, J., Worasuwannarak, N., 2012. Upgrading of woody biomass by

451 torrefaction under pressure. J. Anal. Appl. Pyrolysis 96, 173–180.
452 38. Wei, L., Zhang, L., Xu, S., 2011. Effects of feedstock on co-pyrolysis of biomass and
453 coal in a free-fall reactor. J. Fuel Chem. Technol. 39, 728–734.
454 39. Wen, J.-L., Sun, S.-L., Yuan, T.-Q., Xu, F., Sun, R.-C., 2014. Understanding the
455 chemical and structural transformations of lignin macromolecule during torrefaction.
456 Appl. Energy 121, 1–9.
457 40. Yang, D., Zhong, L., Yuan, T., Peng, X., Sun, R., 2013. Studies on the structural
458 characterization of lignin , hemicelluloses and cellulose fractionated by ionic liquid
459 followed by alkaline extraction from bamboo. Ind. Crop. Prod. 43, 141–149.
460 41. Yang, H., Yan, R., Chen, H., Lee, D.H., Zheng, C., 2007. Characteristics of
461 hemicellulose , cellulose and lignin pyrolysis. Fuel 86, 1781–1788.
462 42. Yang, H., Yan, R., Chen, H., Zheng, C., Lee, D.H., Uni, V., V, N.D., March, R. V,
463 Re, V., Recei, M., September, V., 2006. In-depth investigation of biomass pyrolysis
464 based on three major components : hemicellulose , cellulose and lignin. Energy and
465 Fuels 388–393.
466 43. Zhang, Y., Zheng, Y., Yang, M., Song, Y., 2016. Effect of fuel origin on synergy
467 during co-gasification of biomass and coal in CO_2. Bioresour. Technol. 200, 789–794.
468 44. Zhang, Li, L., Tong, D., Hu, C., 2016. Microwave-enhanced pyrolysis of natural algae
469 from water blooms. Bioresour. Technol. 212, 311–317.
470 45. Zhao, X., Chen, J., Chen, F., Wang, X., Zhu, Q., Ao, Q., 2013. Surface
471 characterization of corn stalk superfine powder studied by FTIR and XRD. Colloids
472 Surfaces B Biointerfaces 104, 207–212.

473

474

Figure captions

Figure 1: Determination of X_A by Gaussian curve deconvolution of the (002) band for SB char prepared at 300 °C.

Figure 2. Comparison of the coalification process with biomass char formation in a Van Krevelen Plot.

Figure 3: Correlations between the chemical characteristics of biomass and biomass chars.

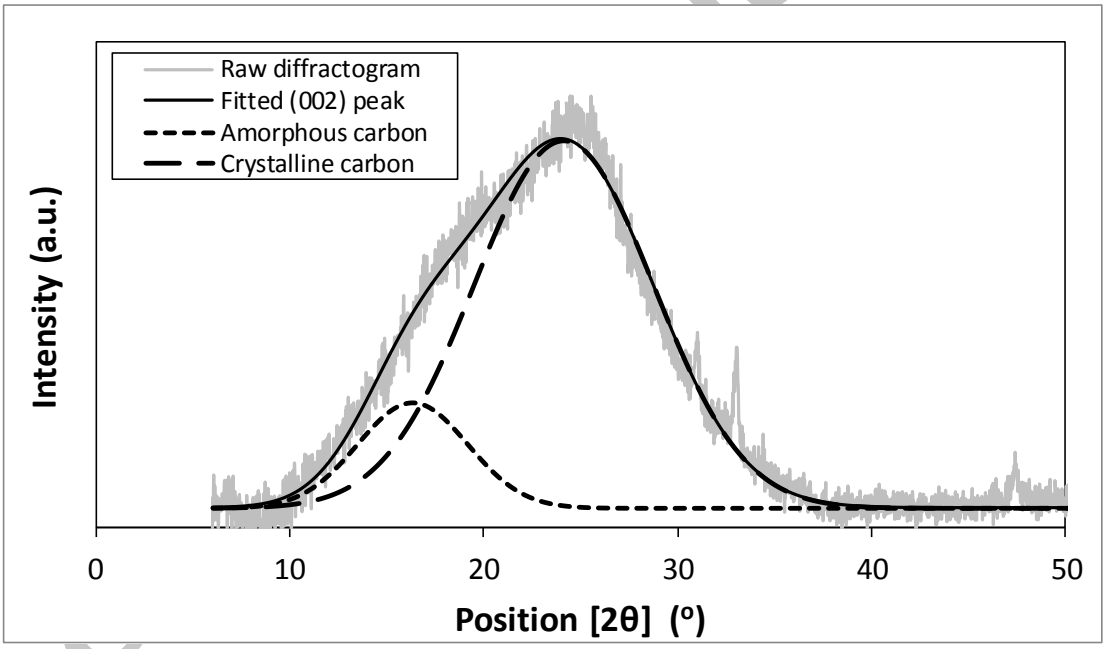

Figure 1: Determination of X_A by Gaussian curve deconvolution of the (002) band for SB char prepared at 300 °C.

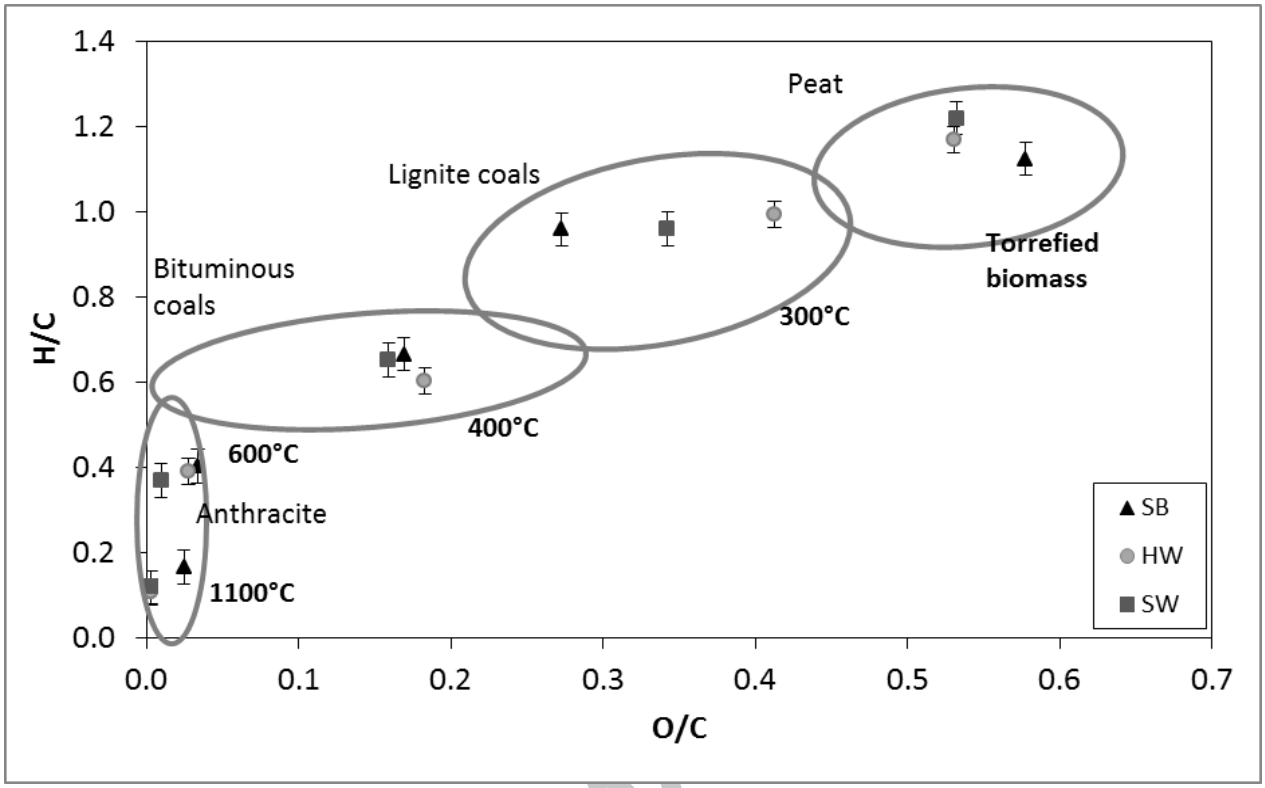

Figure 2. Comparison of the coalification process with biomass char formation in a Van Krevelen Plot.

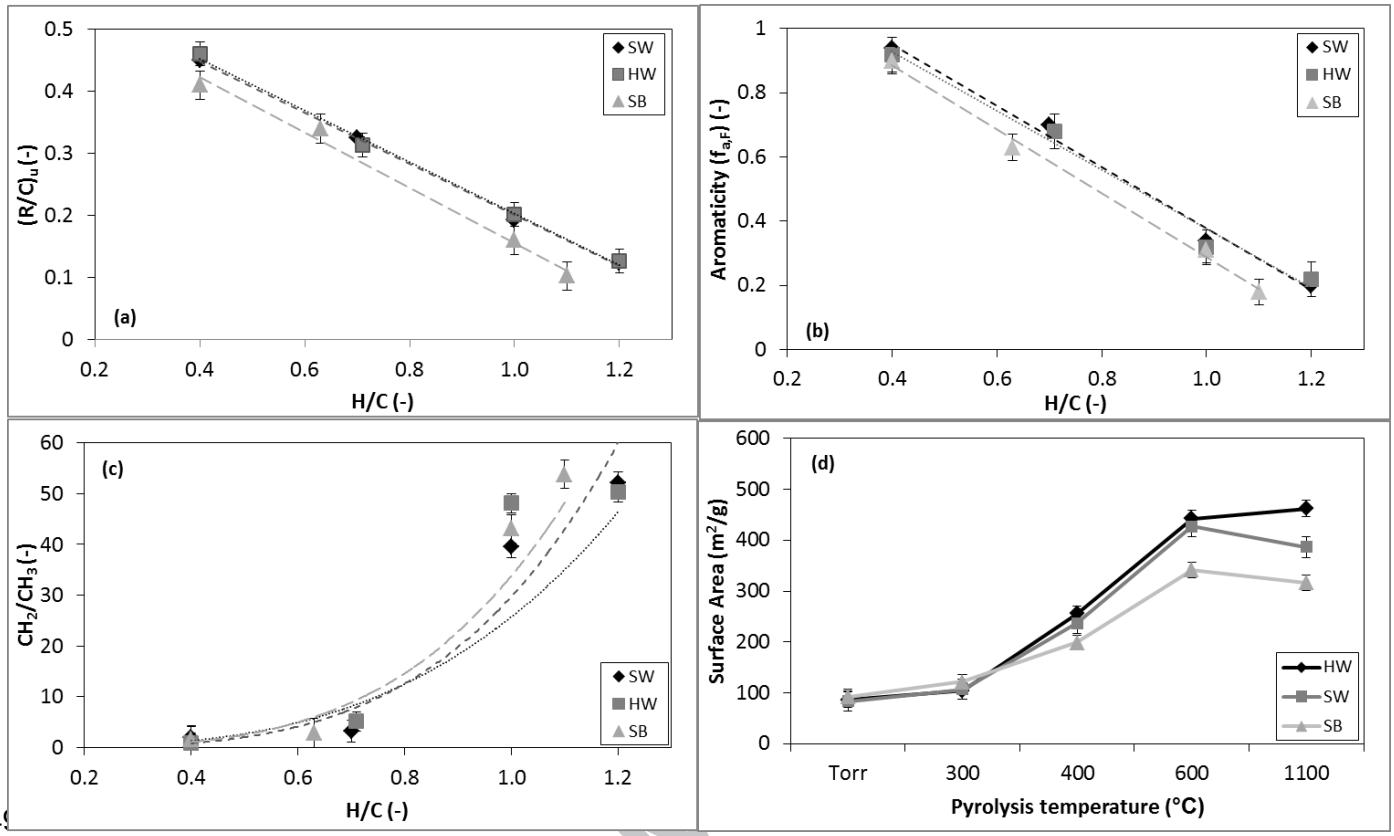

Figure 3: Correlations between the chemical characteristics of biomass and biomass chars.

Table captions

Table 1: Proximate and ultimate analyses for torrefied biomass and chars prepared at different temperatures.

Table 2: Chemical parameters for torrefied biomass and chars.

Table 3: Structural characteristics of torrefied biomass and subsequent chars.

Table 4: Correlation equations of some properties of torrefied biomass and chars.

509 **Table 1:** Proximate and ultimate analyses for torrefied biomass and chars prepared at
510 different temperatures

Sample		Proximate Analysis (wt.%, mfb)				Ultimate Analysis (wt.%, daf)						
		VM[1]	FC[2]	Ash	CV[3] (MJ/kg)	C	H	N	S	O	H/C	O/C
SW	**Torr**	76.5	22.9	0.6	22.3	55.1	5.6	0.13	0.09	39.1	1.2	0.5
	300 °C	63.8	35.5	0.7	23.2	65.2	5.2	nd[4]	0.07	29.7	1.0	0.3
	400 °C	30.7	68.5	0.8	28.8	78.9	4.3	nd	0.06	16.7	0.7	0.2
	600 °C	9.9	89.2	1.0	33.1	95.7	2.9	0.08	0.07	1.2	0.4	0.01
	1100 °C	1.3	97.4	1.2	32.3	99.2	0.6	0.02	0.07	0.06	0.1	0.01
HW	**Torr**	77.3	22.1	0.6	22.4	55.4	5.4	0.01	0.03	39.2	1.2	0.5
	300 °C	64.2	35.3	0.6	23.2	61.2	5.1	nd	0.05	33.7	1.1	0.4
	400 °C	30.4	68.9	0.7	28.1	77.2	3.9	nd	0.04	18.8	0.6	0.2
	600 °C	10.1	89.2	0.8	33.7	93.4	3.0	nd	0.05	3.6	0.4	0.03
	1100 °C	1.2	97.5	1.2	32.1	99.2	0.7	0.03	0.04	0.03	0.1	0.01
SB	**Torr**	69.8	23.7	6.5	23.0	53.4	5.5	0.32	0.15	41.1	1.1	0.6
	300 °C	48.1	45.0	6.8	24.5	69.2	5.0	nd	0.16	25.1	1.0	0.3
	400 °C	26.2	66.1	7.6	26.6	77.9	4.3	0.11	0.15	17.6	0.7	0.2
	600 °C	5.8	82.0	12.2	30.1	92.2	3.1	0.36	0.19	4.2	0.4	0.03
	1100 °C	3.2	83.9	12.5	26.6	97.1	1.3	0.39	0.18	1.0	0.2	0.03

511 [1]VM - volatile matter, [2]FC - fixed carbon and [3]CV - calorific value, [4]nd - not detected

512

513 **Table 2:** Chemical parameters for torrefied biomass and chars.

Sample		Chemical Characteristics			
		$f_{a,N}$	$f_{a,F}$	$(R/C)_u$	CH_2/CH_3 ratio
SW	**Torr**	0.21	0.26	0.12	52.1
	300 °C	0.34	0.37	0.19	39.5
	400 °C	0.71	0.74	0.30	3.2
	600 °C	0.94	0.93	0.48	1.9
	1100 °C	-	-	-	-
HW	**Torr**	0.22	0.24	0.13	50.3
	300 °C	0.32	0.30	0.20	48.1
	400 °C	0.68	0.62	0.31	5.2
	600 °C	0.92	0.92	0.46	1.0
	1100 °C	-	-	-	-
SB	**Torr**	0.18	0.23	0.10	53.8
	300 °C	0.31	0.47	0.16	43.1
	400 °C	0.63	0.63	0.34	2.9
	600 °C	0.90	0.96	0.41	1.6
	1100 °C	-	-	-	-

514
515
516
517
518
519
520
521
522
523
524
525
526
527
528
529

530 **Table 3:** Structural characteristics of torrefied biomass and subsequent chars.

Sample ID		CO_2 adsorption		WA-XRD-CFA					
		S.A (m^2/g)	M.P.V (cm^3/g)	M.P.W (Å)	d_{002} (Å)	L_c (Å)	L_a (Å)	N_{ave} (-)	X_a (-)
SW	**Torr**	83	0.017	3.7	4.0	27	72.0	7.8	0.34
	300 °C	107	0.022	3.6	4.1	19	74	5.6	0.42
	400 °C	236	0.055	3.8	3.9	10	86	3.7	0.21
	600 °C	427	0.092	3.9	3.8	10	125	3.6	0.08
	1100 °C	386	0.083	4.4	3.7	9	139	3.5	-
HW	**Torr**	86	0.018	3.7	4.0	30	65	8.5	0.35
	300 °C	103	0.022	3.6	4.0	17	67	5.2	0.41
	400 °C	255	0.059	3.7	3.9	12	85	4.0	0.18
	600 °C	442	0.094	3.8	3.8	10	115	3.7	0.07
	1100 °C	461	0.097	4.0	3.8	9	130	3.5	-
SB	**Torr**	92	0.02	3.7	4.1	28	69	8.0	0.34
	300 °C	121	0.026	3.6	4.2	17	71	5.0	0.15
	400 °C	198	0.049	3.5	4.0	13	89	4.3	0.06
	600 °C	341	0.073	3.6	3.9	12	135	4.0	-
	1100 °C	316	0.072	3.9	3.8	10	151	3.6	-

531

532

533

534

535

536

537

538

539

540

541

542

543 **Table 4:** Correlation equations of some properties of torrefied biomass and subsequent chars.

Parameter	Sample ID	Correlation equation	R^2
$f_{a,F}$	**SW**	$f_{a,F} = -0.96(H/C) + 1.34$	0.991
	HW	$f_{a,F} = -0.92(H/C) + 1.30$	0.983
	SB	$f_{a,F} = -0.99(H/C) + 1.28$	0.995
$(R/C)_n$	**SW**	$(R/C)_n = -0.41(H/C) + 0.61$	0.998
	HW	$(R/C)_n = -0.42(H/C) + 0.62$	0.997
	SB	$(R/C)_n = -0.44(H/C) + 0.60$	0.990
CH_2/CH_3	**SW**	$CH_2/CH_3 = 26(H/C)^{3.23}$	0.858
	HW	$CH_2/CH_3 = 29.8(H/C)^{3.85}$	0.958
	SB	$CH_2/CH_3 = 33.8(H/C)^{3.74}$	0.924

544

545

546

547

548

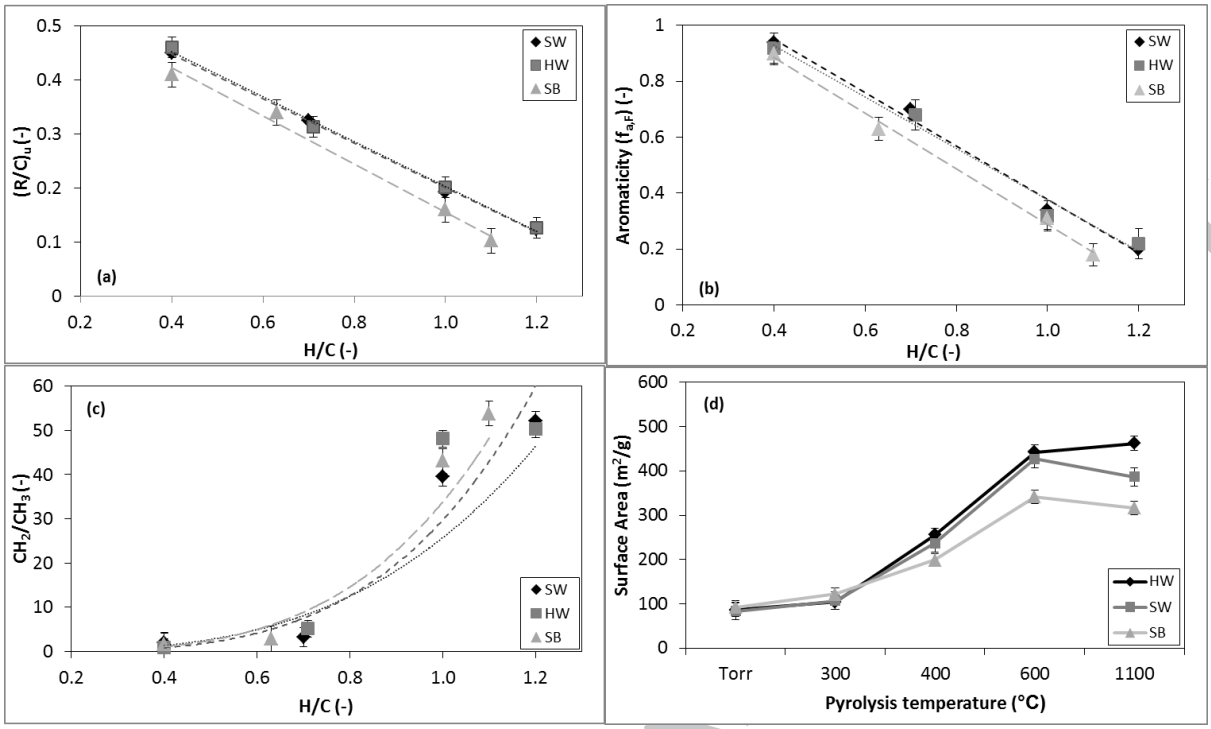

549

550

551 **Highlights**

552 • Lignocellulosic biomass pyrolysis is a 2-step process

553 • Aromaticity can be determined from ATR-FTIR spectroscopy

554 • Aliphatic chains decrease with increasing pyrolysis temperature

555 • The carbon lattice is stretchered into sheets as temperature is increased

556